scientific reports

Check for updates

OPEN

Multimodal imaging of dark without pressure in high myopia reveals evidence that photoreceptor microscopic lesions may be reversible

Qingge Guo[1,2], Xiuxiu Jin[1,2], Xiaoyu Xin[3], Xiaohong Guo[1], Shuai Ming[1,2], Yuxiang Li[3] & Bo Lei[1,2]✉

Dark without pressure (DWP) is the more darkly pigmented area of the retina in the fundus, typically exhibits relatively distinct boundaries, and varies in shape, size, and distribution across different individuals. Previous studies have concluded that DWP alone has no impact visual acuity, visual field, or other visual functions. This study aims to reveal the multimodal imaging manifestations of DWP in high myopia and to explore its impact on retinal function. This is a prospective study. Eleven high myopia patients with DWP were recruited. Detailed ophthalmological examinations, such as visual acuity, intraocular pressure, slit lamp microscope, and fundoscopy, were performed in all participants to exclude other ocular diseases or retinopathies. Multimodal imaging including swept source optical coherence tomography (SS-OCT), adaptive optics (AO) fundus imaging was applied to analyze morphologic manifestations of DWP. Retinal photosensitivity was detected by perimetry or microperimetry. Eight of the participants were followed for at least 5 months and up to 32 months. The DWP appeared as water trace pattern that was darker in color than the surrounding normal fundus. The punctate light reflectivity of the photoreceptor mosaic in AO fundus imaging was missing, and the light reflectivity in ellipsoid zone (EZ) of SS-OCT B scan was attenuated or even disappeared simultaneously. Perimetry revealed reduced retinal photosensitivity in the DWP lesions. At 5-month follow-up, the area of DWP lesions could appear to expand or shrink. Where the DWP faded away, the reflectivity of EZ on SS-OCT returned to normal hyperreflectivity, accompanied with a recovered retinal photosensitivity. The imaging basis for DWP in high myopia is the presence of microscopic lesions in the outer retina which could be shown morphologically with optical imaging and functionally with microperimetry. It is variable in size and may be reversible in function in the fundus.

Keywords Dark without pressure, High myopia, SS-OCT, Cone photoreceptors, Adaptive optics

Abbreviations

DWP	Dark without pressure
SS-OCT	Swept source optical coherence tomography
AO	Adaptive optics
EZ	Ellipsoid zone
FFA	Fundus fluorescein angiography
OCTA	Optical coherence tomography angiography
BCVA	Best-corrected visual acuity
LED	Light emitting diode
cSSO	Confocal scanning superluminescent ophthalmoscopy
NIR	Near-infrared
HFA	Humphrey field analyzer

[1]Henan Eye Institute, Henan Eye Hospital, Henan Provincial People's Hospital, Zhengzhou 450003, China. [2]Eye Institute, Henan Academy of Innovations in Medical Science, 7 Weiwu Road, Zhengzhou, China. [3]Academy of Medical Sciences, Zhengzhou University, Zhengzhou, China. ✉email: bolei99@126.com

SITA	Swedish interactive threshold algorithm
SVC	Superficial vascular complex
ILM	Inner limiting membrane
GCC	Ganglion cell complex
DCP	Deep capillary plexus
INL	Inner nuclear layer
OPL	Outer plexiform layer
ICP	Intermediate capillary plexus
RPE	Retinal pigment epithelium
OS	Outer segment
IPM	Interphotoreceptor matrix
IS	Inner segment
SCE	Stiles–Crawford effect

Dark without pressure (DWP), the more darkly pigmented area of the retina in the fundus, typically exhibits relatively distinct boundaries, and varies in shape, size, and distribution across different individuals[1]. Nagpal et al. defined the term to describe these areas, drawing an analogy with "white without pressure" fundus lesions[2]. It was first identified in the fundus of patients with hematological diseases[3,4]. Subsequently, it has been reported in a range of conditions, including retinal astrocytic hamartoma, multiple evanescent white dot syndrome, uveitis, congenital hypertrophy of the retinal pigment epithelium, Ebola retinal lesions, choroidal osteoma, congenital cataract, Marfan syndrome, and high-risk B acute lymphoblastic leukemia patients' fundus[1,5–8].

The mechanism underlying the pathogenesis of DWP remains unclear. Early investigations falsely assumed that the presence of hemosiderin in the deeper retinal layers, consequent to hemorrhage, or deep subretinal hemorrhage with a central preretinal extension, was responsible[3,4]. Subsequent studies confirmed that DWP is not related to the state of the vitreous, but suggested a possible link with retinal vessel occlusion[2,9]. Steptoe et al. reported that perilesional areas of DWP were present in 88.7% of Ebola retinal lesions, and the extent of DWP appeared to correlate with the density of the Ebola retinal lesions[7]. It has been speculated that DWP may be a secondary manifestation of an ongoing or previous intraretinal stimulus of an infection[10]. Others have also suggested that DWP is an acquired condition that arises during ocular development, rather than being congenital, as it is often associated with pathological changes in the ocular structures, such as high myopia and tumors, while its shape and size could be variable[8,11].

With the rapid advances in ophthalmic examination techniques, especially the application of widefield and ultra-high resolution fundus imaging systems, we now have an opportunity to perform more comprehensive observational research on DWP. Previous studies have concluded that DWP consistently manifested as ellipsoid zone (EZ) hyporeflectivity in optical coherence tomography (OCT) B-scan images, and simple DWP has no impact on visual acuity, visual field, or other visual functions. Abnormal findings are generally not detected with fundus fluorescein angiography (FFA) and optical coherence tomography angiography (OCTA)[1]. However, our recent study of DWP in high myopia has different results in OCTA and visual field from previous, and recorded its reversible evidences in morphological and functionally.

Methods

This prospective study was performed according to the tenets of the Declaration of Helsinki with approval of the Institutional Review Board of Henan Eye Hospital (HNEECKY-2020 (38)). Written informed consent was obtained from each participant.

All subjects were selected from the recruitment of adult high myopia patients. High myopia was diagnosed by comprehensive optometric (negative spherical equivalent ≥ 6.0 D). Eleven high myopia patients with DWP (16 eyes) participated in this study. All participants had the best-corrected visual acuity (BCVA) greater than 1.0 decimals. Two experienced ophthalmologists perform a detailed ophthalmological examinations, such as intraocular pressure, slit lamp microscope, and fundoscopy, were completed to exclude other ocular diseases or retinopathy. The morphologic manifestations of DWP were recorded by multimodal images such as color fundus photography, swept source (SS)-OCT (VG200D, SVision Imaging, Henan, China), and adaptive optics (AO) fundus camera (rtx1, Imagine Eyes, Orsay, France). Retinal photosensitivity was detected by perimetry examination. Eight of the participants were followed for at least 5 months and up to 32 months.

Fundus photography

Fundus photographs were obtained using the ultra-widefield fundus photographs (Optos California, Optos PLC, Dunfermline, United Kingdom), with single viewing angle no less than 200°, and high-definition true-color fundus camera (Clarus 500, Carl Zeiss Meditech, Dublin, CA). The latter using three color light emitting diodes (LEDs) of red (585–640 nm), green (500–585 nm) and blue (435–500 nm), as well as infrared laser diodes (785 nm) to obtain true-color fundus images in the red, green, and blue channel decomposition modes and infrared reflectography. The view angle of a single image was 135° and multiple fundus images can be automatically synthesized into an ultra-widefield montage of up to 267°[12].

SS-OCT

Fundus confocal scanning superluminescent ophthalmoscopy (cSSO), B scan, *En face* and OCTA images were performed using SS-OCT , for which the central wavelength was 1050 nm, and scan speed ≥ 200,000 A-Scan/s. The excitation wavelength of cSSO was 820 nm. OCTA was performed in the 26 mm × 21 mm 1536 × 1240 R2 mode, with each scan containing 1240 B scan lines, and each line containing 1536 A scans, the scan was repeated 2 times. The optical resolution for OCT was 5 μm longitudinally and 20 μm transversely. The digital resolution

of OCTA was 11.719[13,14]. The stratification of the retinal layers was performed automatically by the embedded algorithm[15]. Retinal vascular density was analyzed through stratified segmentation, with the superficial vascular complex (SVC) defined as extending from 5 μm above the inner limiting membrane (ILM) to the outer third of the ganglion cell complex (GCC), while the deep capillary plexus (DCP) encompassed the region from the midpoint of the inner nuclear layer (INL) to 25 μm below the INL/outer plexiform layer (OPL) interface. The intermediate capillary plexus (ICP) occupied the space between these two vascular layers. The outer retina was delineated as the area spanning from 25 μm below the INL/OPL junction to 10 μm above the retinal pigment epithelium (RPE). Two experienced physicians determined the accuracy of the stratification, and manually rectified incorrect stratification when needed.

AO fundus imaging

AO fundus camera imaging system used en face reflectance imaging with noncoherent near-infrared illumination, and the captured single image was 4° × 4° field of view[13,16,17]. The equivalent pixel spacing was 1.1 μm, and optical resolution was 250 line pairs/mm. The system featured a refractive error pre-compensation range of -12 D to + 6 D and a focus adjustment range of ± 800 μm. During image acquisition, refractive errors were first corrected, followed by depth fine-tuning to optimize cone mosaic visibility. By adjusting the fixation target through retina vascular pattern of fundus photographs and SS-OCT cSSO images, to localize the DWP area and capture cone mosaic images.

Static perimetry

Patients with extensively distributed DWP close to the macula were selected for 30° and 60° Humphrey field analyzer (HFA 3 840, Carl Zeiss Meditec, Jena, Germany) and microperimetry (MP-3, Nidek, Japan) examinations[18,19]. The HFA 3 examinations were performed setting 31.5 asb background illumination, Goldman III white light, and Swedish interactive threshold algorithm (SITA) Standard program. The MP-3 examinations were performed settings 31.4 asb background illumination, Goldman III white light, and 4–2 (fast) strategy. The detection points were personalized set near the DWP boundary manually.

Results

Among the eleven subjects, there were five males (eight eyes) and six females (eight eyes), with an average age of 25.47 ± 2.49. Demographic data are shown in Table 1. In these high myopia patients, DWP was mostly located in the mid-peripheral retina and did not affect macula. It appeared as water trace pattern that was darker in color than the adjacent normal fundus (Fig. 1). While most DWP showed sharp and clear boundary, some presented with blurred transitions on the boundary. The shape of DWP varied, could manifest in a fan-shape or irregular pattern in a large and extensive area.

Multimodal imaging manifestations of DWP

DWP could be identified easily in true-color and ultra-widefield fundus photographs (Fig. 1 A-D and E, Fig. 2A), including red channel and red-free channel (Fig. 2 B and C), as well as cSSO images of SS-OCT (Fig. 2D). Compared with the red channel, it was clearer in red-free imaging. In SS-OCT B-scan, the EZ hyper-reflectivity showed attenuation or even disappearance corresponding to the DWP area, with the choroidal vessels dilated (Fig. 2E). In AO fundus imaging, it showed loss of punctate reflectivity of the cone photoreceptors mosaic in DWP region (Fig. 2F).

Patient ID	Age (years)	Gender	Eye	SER(D)	AL(mm)	Fundus images
1	23	F	OD	−6.00	27.22	Figure 1A, E; Fig. 3A–F
1	23	F	OS	−6.00	27.20	Figure 2A, B, C; Fig. 4C1–C4
2	23	M	OD	−8.75	28.19	Figure 2D, E, F; Fig. 4 B1, B2
2	23	M	OS	−8.50	28.46	Figure 1D
3	24	F	OD	−9.25	25.48	
4	24	F	OD	−6.00	25.81	Figure 4A1, A2
5	24	F	OD	−7.25	26.84	Figure 2G–L
5	24	F	OS	−8.25	27.40	
6	24	M	OD	−8.25	28.35	
6	24	M	OS	−7.25	27.85	
7	25	M	OD	−6.00	26.75	
7	25	M	OS	−7.00	26.98	
8	25	F	OS	−9.00	26.26	
9	27	M	OD	−6.50	26.83	Figure 1B
10	27	M	OS	−9.00	27.31	
11	32	F	OD	−7.25	25.19	Figure 1C

Table 1. Demographic data of high myopia patients with dark without pressure. SER, spherical equivalent refraction; AL, axial length; F, female; M, male; OD, right eye; OS, left eye.

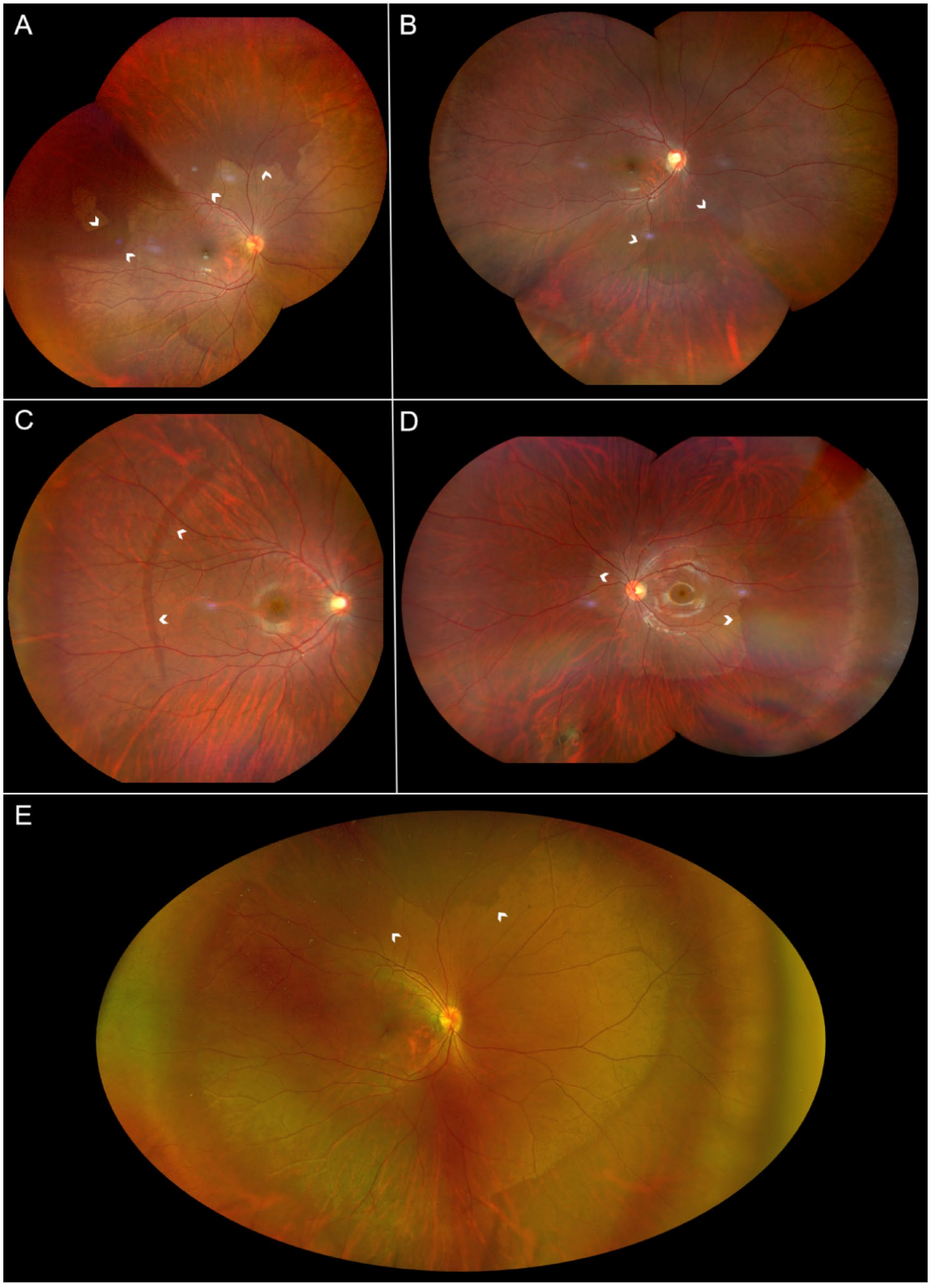

Fig. 1. The manifestation of dark without pressure (DWP) in high myopia fundus. (**A**–**D**) True-color fundus photographs from four representative patients show DWP lesions as irregular, water-track-like areas with distinct borders (demarcated by white arrows). (**E**) ultra-widefield follow-up photograph at 27 months demonstrates dynamic changes in lesion morphology in the same patient as panel (**A**).

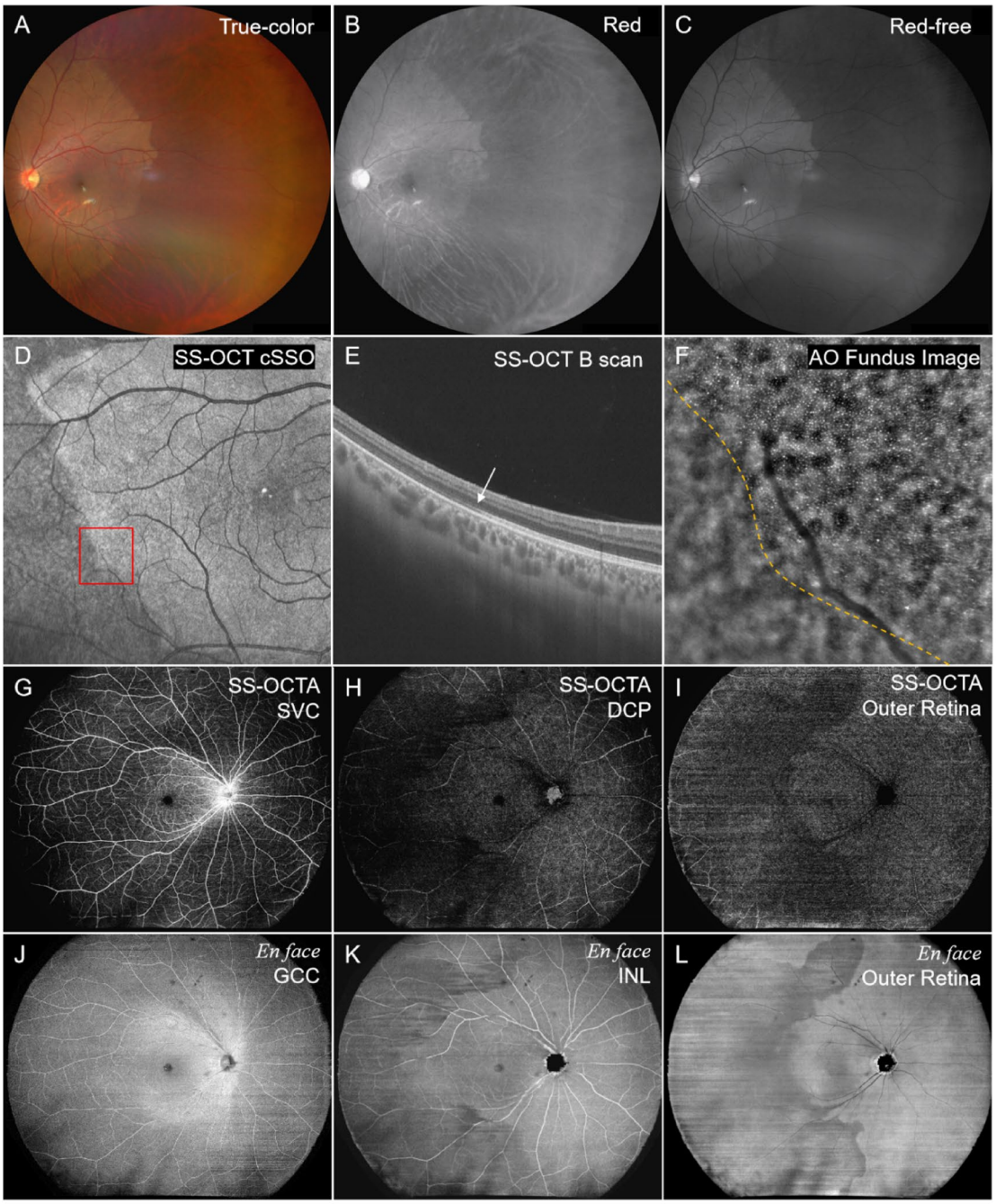

Fig. 2. Multimodal imaging features of DWP. (**A**–**C**) Fundus photographs demonstrate DWP as darker areas in true-color, red channel, and red-free imaging. (**D**) Swept-source optical coherence tomography (SS-OCT) confocal scanning superluminescent ophthalmoscopy (cSSO) image. (**E**) SS-OCT horizontal B scan (red box in panel **D**) shows disappearance of ellipsoid zone (EZ) and interdigitation zone reflective signals in the DWP region (left of white arrow), with dilated choroidal vessels. (**F**) Adaptive optics (AO) fundus image (red box in panel **D**) demonstrates loss of cone masic reflectance in the DWP area (left of yellow dashed line). (**G**–**I**) Optical coherence tomography angiography (OCTA) images. Vascular perfusion in the DWP region remains intact in the superficial vascular complex (SVC) layer, but is significant reduced in both the deep capillary plexus (DCP) and outer retinal layer. (**J**–**L**) *En face* SS-OCT images. Reflectivity of DWP lesion is unchanged in the ganglion cell complex (GCC) layer, slightly decreased in the inner nuclear (INL) layer, and markedly reduced in the outer retinal layer.

In SS-OCTA imaging, there was no obvious change of the SVC (Fig. 2G) and ICP slab in the inner retina. However the DCP (Fig. 2H) and the outer retina (Fig. 2I) layers' blood perfusion were reduced in different degrees. And there was a slight increase in the choriocapillary layer. In SS-OCT *En face* imaging, DWP presented a corresponding hyporeflective mainly in the outer retinal layer, while no obvious changes in the GCC layer. The INL was intermediate between these two cases, showing slight variations (Fig. 2J–L).

DWP lesions could expand or shrink over time. Where the DWP faded away, the reflectivity of EZ on SS-OCT also returned to normal hyperreflectivity (Fig. 3).

Changes of retinal photosensitivity

In function tests, four eyes completed 30° HFA, eight eyes completed 60° HFA, and two eyes completed microperimetry. From the greyscale map of HFA, slightly decreased areas of retinal photosensitivity roughly overlapped with the DWP lesion areas. At a maximum follow-up of 32 months, retinal photosensitivity also recovered in areas where DWP had resolved (Fig. 4).

Discussion

DWP is characterized by relative dark areas in fundus photographs (including red, red-free, and full color), and fine abnormalities in SS-OCT cSSO, and *En face* images. Although affected by variations related to the fundus site and pigmentation, the fundus reflectance is low at the short wavelengths (445 nm) and high at long wavelengths (> 640 nm). The fundus has a pronounced reflectance between 790 and 1070 nm, and no reflectance above 1200 nm[20].

Using an ultra-high resolution AO fundus imaging system, we observed the disappearance of cone reflectivity in the DWP lesions area of the myopic eyes. This might be the reason that DWP appeared in dark appearance in the fundus. The underlying mechanisms of this phenomenon are unclear, but the reflectivity changes in cone photoreceptors may be related to the alterations themselves or their surrounding micro-environments[21,22]. Its

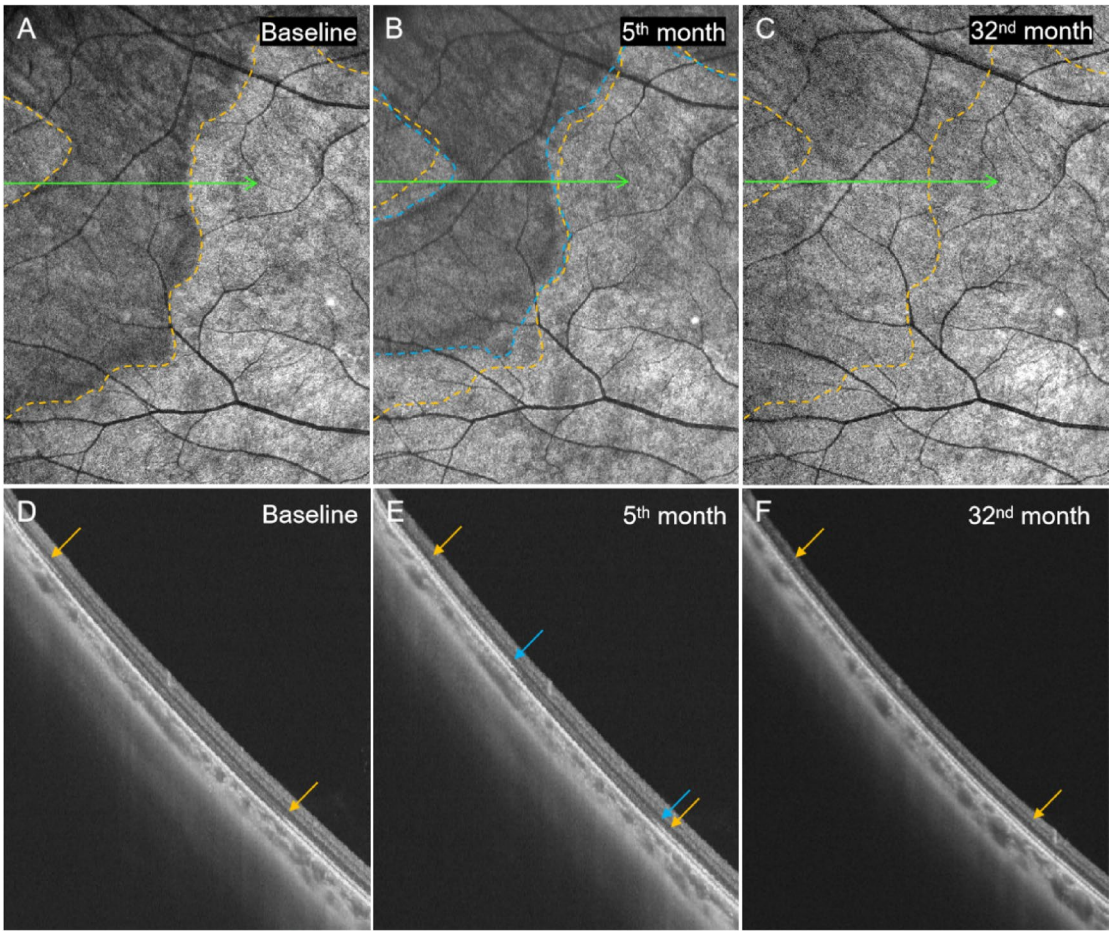

Fig. 3. SS-OCT follow-up imaging of DWP progression. (**A**–**C**) cSSO imaging at baseline, 5-month, and 32-month follow-up. The DWP area changes over time, either expanding or contracting, and almost disappeared at the 32-month. Yellow dashed lines indicate the initial DWP bondary; blue dashed lines mark the 5-month follow-up boundary. (**D**–**F**) B scan images (green lines in panels **A**–**C**). Yellow arrows denote the initial DWP boundary; blue arrows indicate the 5-month boundary. In the DWP lesion regressed area (**F**), EZ reflective signals recover to normal hyperreflectivity.

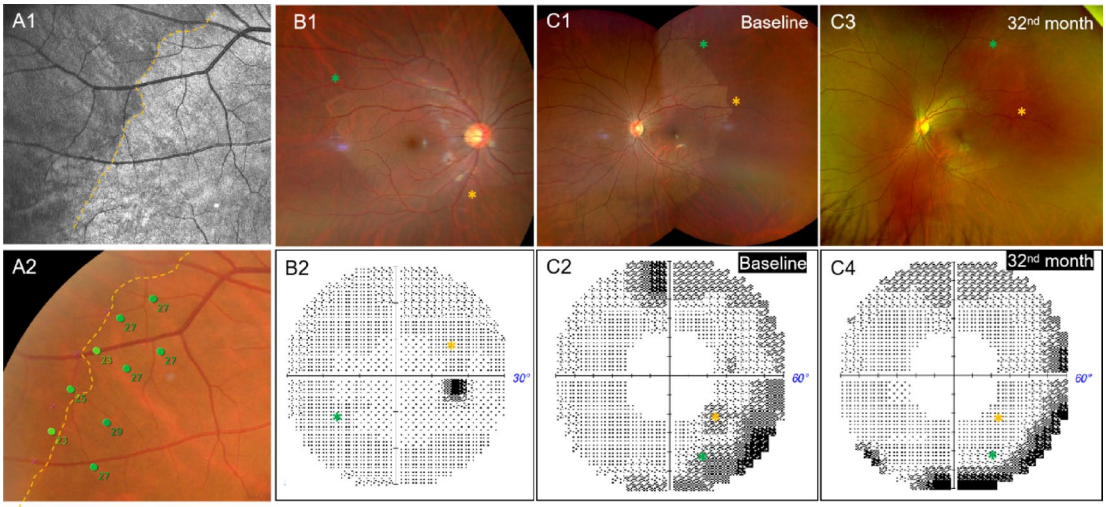

Fig. 4. Retinal photosensitivity changes associated with DWP. (**A**1, **A**2) cSSO image and microperimetry results of patient 4. Yellow dashed lines indicate the DWP boundary. Green dots mark test locations and near numbers indicating photosensitivity thresholds (dB). The DWP region shows a 2–4 dB reduction in retinal sensitivity (one vessel-associated point excluded). (**B**1, **B**2) Fundus photographs and 30° visual field greyscale map of patient 2. The DWP area display a midly decreased retinal photosensitivity. Colored asterisks denote corresponding anatomical positions. (**C**1–**C**4) Fundus photographs and 60° visual field greyscale maps of patient 1 before and after 32-month follow-up. Regression of DWP in the temporal superior retina (asterisks marked) correlates with partial recovery of photosensitivity.

known that, subtle changes in the length of the outer segment (OS) caused by the daily renewal and shedding of OS discs can lead to alternating light and dark changes in the reflectivity of individual cones[23–25]. Alterations in disc membrane properties due to changes in disc-to-disc spacing can lead to variations in the waveguide properties of photoreceptors[26], spatial variations in the absorptivity of cone photopigments[21] changes in the chemical composition of the interphotoreceptor matrix (IPM)[27], and optical interference effects, which may cause changes in cone reflectance over time[28].

In SS-OCT B scan, DWP areas showed EZ hyporeflectivity, which is consistent with previous studies[1]. Due to differences in the refractive index, the various layers of retinal tissue appeared as reflective bands of varying brightness in the OCT B scan. EZ, the second hyperreflective band of the outer retina, represents the structural and functional integrity of the mitochondria in photoreceptors[29,30]. Changes in reflection may indicate pathological or metabolic changes within the organelles, such as mitochondria, leading to a decline of photoreceptor function[29,31,32]. For example, patients with autosomal recessive Oguchi disease present with a golden yellow reflex fundus due to abnormal retinoid pigments circulation in the retinal photoreceptor cells. The fundus may return to normal appearance after prolonged dark adaptation, i.e., the Mizuo-Nakamura phenomenon, and the EZ would return to normal from hyperreflectivity[33,34]. From this, we speculate that the attenuation or even disappearance of the EZ reflectivity in the DWP of the high myopic could be associated with retinal abnormalities, including morphological structure changes of the cone photoreceptors.

DWP rarely involves the macula. Although DWP is primarily distributed in the retina dominated by rods, it is believed to be associated with alterations in cone photoreceptor imaging. This is because the boundaries are sharp and clear in the mesial margin where cones still exist, whereas the peripheral areas with fewer cones mostly have blurred transitions. Additionally, rods have a smaller IS and lower mitochondrial density than cones, making them difficult to image with current OCT and AO technologies. It is known that the reflection of light from interfaces of the IS/OS and the OS/retinal pigment epithelium corresponds to the EZ and interdigitation zones (the third hyperreflective zone of the outer retina), respectively[21]. By changing the direction of the incident light, the reflection intensity of the interdigitation zone can be altered due to the Stiles-Crawford effect (SCE)[35]. Cones can also maintain the rectilinearity of the IS and OS due to the SCE, which is almost absent in rods[36,37]. Chai et al. found that the murine photoreceptor IS's orientation undergoes light-dependent movement, but the OS has a seemingly light-independent orientation. The different orientations of the IS and OS gave rise to the non-rectilinearity of the photoreceptors, but this did not affect function[36]. In addition, the IS misalignment may involves mechanical forces extrinsic to the photoreceptors caused by the cellular motility such as Müller glial cell[36]. Ball et al. found that the cone directional sensitivity is dependent on the effective mitochondrial refractive index, which can be changed depending on respiration state and protein concentration. The active mitochondria, which are elongated and tightly packed, have a larger refractive index. However, light stimulation during childhood permanently determines the orientation of the photoreceptors to a large extent[29]. Wilson et al. indicated that isolated mitochondria contribute significantly to light scattering in the range of 5–90°, and mitochondrial swelling caused by oxidative stress resulted in significant changes in angle-resolved scattering[38]. On the other hand, Yu et al. showed that longer axial length was a risk factor for DWP[39]. Taking together, we propose that the DWP of high myopia may be related to the decreased light reflectance of cones, which may be

caused by the abnormal morphology or function of mitochondria due to mechanical forces in the process of eye axial elongation.

Previous studies have suggested that DWP does not affect visual acuity or visual fields[1]. However, we found that DWP of high myopia lead to a decrease in the photosensitivity of the corresponding retina. This was based on the face that the grayscale maps in perimetry were almost exactly corresponding to the DWP areas, and the retinal photosensitivity recovered in the diminished DWP area after a long-term followed-up. The MP-3 microperimetry's restricted testing range (± 20°) confined our evaluation to macular-proximal DWP lesions. For peripheral lesions, we relied on HFA-derived visual fields, interpreting defect locations through established retinotopic mapping principles (superior visual field corresponds to the inferior retina), though this method's spatial precision is inherently limited by the absence of fundus tracking.

Although cone reflectance is an indicator of retinal health, the absence of cone reflection signals in OCT or AO fundus imaging does not necessarily indicate that cones are absent or non-functional[28]. Some studies have shown that cones positioned directly in the shadow of the retinal vessels have decreased photosensitivity, and those in the penumbra also experienced changes in the photosensitivity[40]. In Idiopathic Macular Telangiectasia Type II, an early onset of the outer retinal disease, cone reflection is diminished or lost, but these cones may regain their normal scattering properties over time, as demonstrated by AO microperimetry and/or OCT images. It suggested that cones with abnormal OS experience a loss of visibility but not necessarily a complete loss of function[41]. Tu et al. reported that a patient with acute bilateral foveolitis showed a reduced but measurable sensitivity threshold in the area of apparent cone loss within the fundus lesion[42]. Another study confirmed the presence of microscopic spots in the retina of a patient with middle-wavelength-sensitive cone mutations resulting in the disruption of the cone mosaic. Although an estimated 30% of the cone photoreceptors were damaged, the dichromatic patient had normal visual acuity and visual field, suggesting that small spot perimetry may be necessary to determine the functional impact of subtle changes in the photoreceptors. It has recently been observed in some non-human primates that permanent shadows result in a form of local amblyopia involving only a few cones[43]. Thus, comparative studies of the microscopic morphology and function may be of greater significance. Currently, non-invasive visualization of cones using two-photon autofluorescence imaging[44], or the non-invasive detection of scattering changes in the retinal tissue using NIR without initiating phototransduction, have been conducted[45]. These in-coming technological advancements may provide an in-depth understanding towards DWP.

This study has two main limitations in retinal function assessment: (1) potential measurement bias from subjective testing methods, and (2) wide-field perimetry (160–180°) demonstrated reduced reliability in high myopia due to optical distortions from corrective lenses and posterior scleral staphyloma.

In conclusions, DWP in high myopia represents the attenuation of light reflective signals of retinal photoreceptor in SS-OCT and AO imaging, accompanied by a decrease in photosensitivity. It was observed to be reversible. Its imaging basis might lie on the presence of microscopic lesions in the outer retina.

Data availability

The data of this study are available from the corresponding author upon reasonable request.

Received: 13 August 2024; Accepted: 20 May 2025
Published online: 29 May 2025

References

1. Fawzi, A. A. et al. Multimodal imaging of white and dark without pressure fundus lesions. *Retina* **34**(12), 2376–2387 (2014).
2. Nagpal, K. C. et al. Dark-without-pressure fundus lesions. *Br. J. Ophthalmol.* **59**(9), 476–479 (1975).
3. Condon, P. I. & Serjeant, G. R. Ocular findings in homozygous sickle cell anemia in Jamaica. *Am. J. Ophthalmol.* **73**(4), 533–543 (1972).
4. Condon, P. I. & Serjeant, G. R. Ocular findings in hemoglobin SC disease in Jamaica. *Am. J. Ophthalmol.* **74**(5), 921–931 (1972).
5. Chang, M. Y. et al. "Shadow sign" in congenital hypertrophy of the retinal pigment epithelium of young myopic pigmented patients. *Eye (Lond.)* **30**(1), 160–163 (2016).
6. Li, M. M., Dalvin, L. A. & Shields, C. L. Coexisting white and dark without pressure abnormalities surrounding congenital hypertrophy of the retinal pigment epithelium. *J. Pediatr. Ophthalmol. Strabismus* **56**, e5–e7 (2019).
7. Steptoe, P. J. et al. Multimodal imaging and spatial analysis of ebola retinal lesions in 14 survivors of ebola virus disease. *JAMA Ophthalmol.* **136**(6), 689–693 (2018).
8. Sherman, T. et al. Dark without pressure in a case of choroidal osteoma. *Retina Cases Brief Rep.* **16**(5), 593–596 (2020).
9. Talbot, J. F. et al. Sickle cell retinopathy in Jamaican children: Further observations from a cohort study. *Br. J. Ophthalmol.* **72**(10), 727–732 (1988).
10. Steptoe, P. J., Beare, N. & Semple, M. G. Comment on: Dark without pressure retinal changes in a paediatric age group. *Eye (Lond.)* **35**(11), 3163–3164 (2021).
11. Flores, P. M. et al. Dark without pressure retinal changes in a paediatric age group. *Eye (Lond.)* **35**(4), 1221–1227 (2021).
12. Matsui, Y. et al. Comparisons of effective fields of two ultra-widefield ophthalmoscopes, optos 200Tx and clarus 500. *Biomed. Res. Int.* **2019**, 7436293 (2019).
13. Xin, X. et al. High-resolution image analysis reveals a decrease in lens thickness and cone density in a cohort of young myopic patients. *Front. Med. (Lausanne)* **8**, 796778 (2021).
14. Zhou, N. et al. Appearance of tumor vessels in patients with choroidal osteoma using swept-source optical coherence tomographic angiography. *Front. Oncol.* **11**, 762394 (2021).
15. Gao, Y. et al. Retinal microvascular changes in white matter hyperintensities investigated by swept source optical coherence tomography angiography. *BMC Ophthalmol.* **22**(1), 77 (2022).
16. Chew, A. L. et al. Agreement in cone density derived from gaze-directed single images versus wide-field montage using adaptive optics flood illumination ophthalmoscopy. *Transl. Vis. Sci. Technol.* **6**(6), 9 (2017).
17. Zaleska-Zmijewska, A. et al. Human photoreceptor cone density measured with adaptive optics technology (rtx1 device) in healthy eyes: Standardization of measurements. *Medicine (Baltimore)* **96**(25), e7300 (2017).

18. Lin, F. et al. Classification of visual field abnormalities in highly myopic eyes without pathologic change. *Ophthalmology* **129**(7), 803–812 (2022).
19. Balasubramanian, S. et al. Interdevice comparison of retinal sensitivity assessments in a healthy population: the CenterVue MAIA and the Nidek MP-3 microperimeters. *Br. J. Ophthalmol.* **102**(1), 109–113 (2018).
20. Delori, F. C. & Pflibsen, K. P. Spectral reflectance of the human ocular fundus. *Appl. Opt.* **28**(6), 1061–1077 (1989).
21. Pallikaris, A., Williams, D. R. & Hofer, H. The reflectance of single cones in the living human eye. *Invest. Ophthalmol. Vis. Sci.* **44**(10), 4580–4592 (2003).
22. Masella, B. D., Hunter, J. J. & Williams, D. R. New wrinkles in retinal densitometry. *Invest. Ophthalmol. Vis. Sci.* **55**(11), 7525–7534 (2014).
23. Putnam, N. M. et al. Modeling the foveal cone mosaic imaged with adaptive optics scanning laser ophthalmoscopy. *Opt. Express* **18**(24), 24902–24916 (2010).
24. Kocaoglu, O. P. et al. Photoreceptor disc shedding in the living human eye. *Biomed. Opt. Express* **7**(11), 4554–4568 (2016).
25. Hillmann, D. et al. In vivo optical imaging of physiological responses to photostimulation in human photoreceptors. *Proc. Natl. Acad. Sci. U S A* **113**(46), 13138–13143 (2016).
26. Marcos, S., Burns, S. A. & He, J. C. Model for cone directionality reflectometric measurements based on scattering. *J. Opt. Soc. Am. A Opt. Image Sci. Vis.* **15**(8), 2012–2022 (1998).
27. DeLint, P. J. et al. Slow optical changes in human photoreceptors induced by light. *Invest. Ophthalmol. Vis. Sci.* **41**(1), 282–289 (2000).
28. Bensinger, E., Wang, Y. & Roorda, A. Patches of dysflective cones in eyes with no known disease. *Invest. Ophthalmol. Vis. Sci.* **63**(1), 29 (2022).
29. Ball, J. M., Chen, S. & Li, W. Mitochondria in cone photoreceptors act as microlenses to enhance photon delivery and confer directional sensitivity to light. *Sci. Adv.* **8**(9), n2070 (2022).
30. Spaide, R. F. & Curcio, C. A. Anatomical correlates to the bands seen in the outer retina by optical coherence tomography: literature review and model. *Retina* **31**(8), 1609–1619 (2011).
31. Wilson, J. D., Cottrell, W. J. & Foster, T. H. Index-of-refraction-dependent subcellular light scattering observed with organelle-specific dyes. *J. Biomed. Opt.* **12**(1), 14010 (2007).
32. Cuenca, N., Ortuno-Lizaran, I. & Pinilla, I. Cellular characterization of OCT and outer retinal bands using specific immunohistochemistry markers and clinical implications. *Ophthalmology* **125**(3), 407–422 (2018).
33. Takada, M. et al. Spectral-domain optical coherence tomography findings in the Mizuo-Nakamura phenomenon of Oguchi disease. *Retina* **31**(3), 626–628 (2011).
34. Pilotto, E. et al. Two novel compound heterozygous SAG mutations in an Italian patient with Oguchi disease: A genetic and multimodal retinal imaging study. *Eur. J. Ophthalmol.* **32**, 484528094 (2021).
35. Curcio, C. A. et al. Cellular characterization of OCT and outer retinal bands using specific immunohistochemistry markers and clinical implications. *Ophthalmology* **125**(7), 407–422 (2018).
36. Chai, Z. et al. Light-dependent photoreceptor orientation in mouse retina. *Sci. Adv.* **6**(51), eabe2782 (2020).
37. Westheimer, G. Directional sensitivity of the retina: 75 years of Stiles-Crawford effect. *Proc. Biol. Sci.* **275**(1653), 2777–2786 (2008).
38. Wilson, J. D. et al. Light scattering from intact cells reports oxidative-stress-induced mitochondrial swelling. *Biophys. J.* **88**(4), 2929–2938 (2005).
39. Yu, H. et al. Analysis of white and dark without pressure in a young myopic group based on ultra-wide swept-source optical coherence tomography angiography. *J. Clin. Med.* **11**(16), 4830 (2022).
40. Spitschan, M., Aguirre, G. K. & Brainard, D. H. Selective stimulation of penumbral cones reveals perception in the shadow of retinal blood vessels. *PLoS ONE* **10**(4), e124328 (2015).
41. Wang, Q. et al. Adaptive optics microperimetry and OCT images show preserved function and recovery of cone visibility in macular telangiectasia type 2 retinal lesions. *Invest. Ophthalmol. Vis. Sci.* **56**(2), 778–786 (2015).
42. Tu, J. H. et al. Dysflective cones: Visual function and cone reflectivity in long-term follow-up of acute bilateral foveolitis. *Am. J. Ophthalmol. Case Rep.* **7**, 14–19 (2017).
43. Tuten, W. S., Tiruveedhula, P. & Roorda, A. Adaptive optics scanning laser ophthalmoscope-based microperimetry. *Optom. Vis. Sci.* **89**(5), 563–574 (2012).
44. Sharma, R. et al. Two-photon autofluorescence imaging reveals cellular structures throughout the retina of the living primate eye. *Invest. Ophthalmol. Vis. Sci.* **57**(2), 632–646 (2016).
45. Jonnal, R. S. et al. In vivo functional imaging of human cone photoreceptors. *Opt. Express* **15**(4), 16141–16160 (2007).

Acknowledgements

The authors thank the study participants, and grateful to the Dr. Qianqian Shi at Henan Eye Hospital for the help in the fundus photographs.

Author contributions

QG designed, performed the experiments, and wrote the original draft of the manuscript. X.J. supervised the project and reviewed the manuscript. X.X., X.G., and Y.L. performed the experiments and collected the data. SM contributed to data analysis. BL conceived the experiments and reviewed the manuscript. All authors read and approved the final manuscript.

Funding

Henan Provincial Science and Technology Research Project (212102310308). National Natural Science Foundation of China (82271084).

Declarations

Competing interests

The authors declare no competing interests.

Additional information

Correspondence and requests for materials should be addressed to B.L.

Reprints and permissions information is available at www.nature.com/reprints.